Resonant nuclear Bragg diffraction from epitaxial 57Fe2O3 on natural Fe2O3

J. Z. Tischler and B. C. Larson

Citation: Journal of Applied Physics **70**, 7532 (1991); doi: 10.1063/1.349705
View online: http://dx.doi.org/10.1063/1.349705
View Table of Contents: http://scitation.aip.org/content/aip/journal/jap/70/12?ver=pdfcov
Published by the AIP Publishing

Resonant nuclear Bragg diffraction from epitaxial $^{57}Fe_2O_3$ on natural Fe_2O_3

J. Z. Tischler and B. C. Larson
Solid State Division, Oak Ridge National Laboratory, Oak Ridge, Tennessee 37831-6030

(Received 4 June 1991; accepted for publication 1 September 1991)

We have used a ^{57}Co Mössbauer source to measure the resonant nuclear scattering properties of epitaxial $^{57}Fe_2O_3$ grown on natural Fe_2O_3 substrates. Isotopically enriched $^{57}Fe_2O_3$ layers were grown on ⟨111⟩ oriented Fe_2O_3 by chemical vapor transport; Mo $K\alpha$ rocking curve measurements showed the mosaic spread of the epitaxial layers to be ~ 15 arcs. The resonant nuclear scattering properties were characterized by absolute integrated intensity measurements of the (electronic and nuclear resonant) 666 reflection and the (pure nuclear resonant) 777 reflection as a function of energy near the resonance. The energy widths of the diffracted intensities were found to be ~ 40 neV ($\sim 10\Gamma$) and the integrated intensities were found to lie between the values calculated from kinematic and dynamic diffraction theories. The results indicate that epitaxial crystals such as these can be used for resonant nuclear monochromators to obtain resonant x-ray beams from synchrotron sources.

I. INTRODUCTION

The continuous energy spectrum generated by synchrotron x-ray sources provides the possibility of obtaining high brightness x-ray beams with submicrovolt energy resolution through the use of resonant nuclear (Mössbauer) scattering. The theory of resonant nuclear Bragg scattering from crystals has been extensively investigated,[1–5] and experimental measurements using radioactive Mössbauer sources[6–13] have verified the major features of the theory. As a result, a basis for extracting beams of Mössbauer resonant photons from the continuous x-ray spectrum of synchrotron sources is available using a number of techniques, in particular, electronically forbidden superstructure reflections.[1,5] Resonant beams of a few tens of photons/second have been obtained using synchrotron bending magnets and wigglers,[14–16] and ~ 500 photons/s has been reported using an undulator.[17] Through further work on optimizing the diffraction techniques and through the use of more intense primary beams expected from undulators in future synchrotron light sources, it is anticipated that beams $\sim 10^5$ photons/s will be obtained.

In order to circumvent the need for bulk quantities of pure isotopes in Mössbauer monochromators, we have grown thin epitaxial layers of enriched $^{57}Fe_2O_3$ on natural Fe_2O_3 crystals and investigated the resonant scattering properties of these crystals. We discuss the method of growth and present absolute integrated intensity measurements of resonant nuclear scattering using a laboratory ^{57}Co Mössbauer source, which demonstrate that high quality crystals of resonantly scattering $^{57}Fe_2O_3$ can be produced by epitaxial growth on natural Fe_2O_3 crystals.

II. EXPERIMENT

Epitaxial layers of enriched $^{57}Fe_2O_3$ were grown on low mosaic width natural Fe_2O_3 single crystals using chemical vapor transport.[18,19] Fe_2O_3 substrates of dimensions $\sim 10\times 20\times 1$ mm^3 with ⟨111⟩ surface normals were cut from a single crystal of natural hematite, mechanically polished, and then etched with hydrochloric acid to remove mechanically induced surface damage. The mosaic spread of these substrate crystals was measured to be 8 arcs using a double crystal diffractometer (Mo $K\alpha$ radiation and a Si (711) monochromator); x-ray reflection topographs showed the substrates to be uniform and free from large angle grain boundaries.

As shown schematically in Fig. 1, the substrates were placed on a slightly cooled pedestal inside a sealed fused quartz chamber containing 120 Torr of HCl gas and a 20 mg charge of 80% enriched $^{57}Fe_2O_3$ powder. Chemical vapor transport growth of $^{57}Fe_2O_3$ epitaxially onto the substrate was then accomplished by heating the chamber to 600 °C for a period of 10 days while a stream of air externally cooled the pedestal (and hence the substrate) transporting mass from the charge of $^{57}Fe_2O_3$ powder to the exposed surface of the substrate. Using this procedure, an epitaxial layer of 65% enriched $^{57}Fe_2O_3$ ~ 25 μm thick was grown on the surface of the substrate. The enrichment of the final layer was measured by secondary ion mass spectroscopy (SIMS), and the decrease in enrichment is probably due to transport of natural material from other parts of the substrate to its surface in addition to any diffusion at the surface. Rocking curve measurements showed the resulting $^{57}Fe_2O_3$ layers to be ~ 15 arcs wide over much of the surface with a region near the mechanical hold down position that had widths ~ 35 arcs. In the 15 arcs wide region, the Mo $K\alpha$ integrated intensity of the 666 reflection was measured to be 7×10^{-5}, which lies between the dynamical and kinematic values of 4×10^{-5} and 9×10^{-5}. Visually, the small region near the hold down with the wide rocking curves appeared to have grown faster than the remaining portion of the crystal, and it also contained some large angle grain boundaries. Due to photoelectric absorption alone, the mean depth of diffracted radiation is only 13 μm which is half the thickness of the enriched layer. Since both resonant and dynamical effects will make the effective depth even less than 13 μm, the enriched layer is thick enough for resonant diffraction studies.

The resonant nuclear diffraction properties of the epitaxial $^{57}Fe_2O_3$ crystals were measured using a radioactive

 0021-8979/91/127532-05$03.00

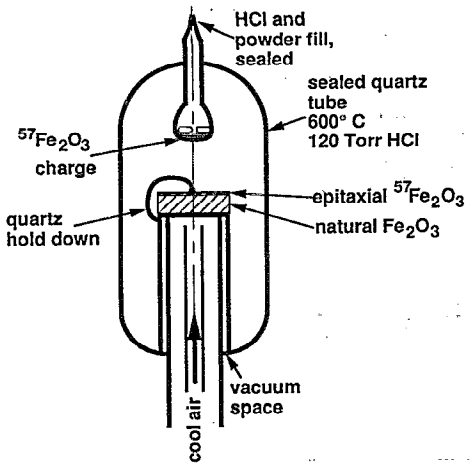

FIG. 1. Apparatus used for growth of the epitaxial crystals.

^{57}Co source in a Rh matrix (5 mm diam, 50 mCi). The experimental setup, including a computer controlled single axis spectrometer, a NaI(T1) scintillation detector, and a multichannel analyzer, is shown schematically in Fig. 2. The ^{57}Co x-ray source was mounted on a Doppler velocity transducer, and the sample angle was varied using a precision rotation stage. Computer control of the velocity transducer was through a programmable function generator; thus, the source velocity as a function of time could be chosen to make optimal use of the available photons. The slits collimating the spectrometer provided an angular resolution of $\sim 0.2°$, for which the intensity of the Mössbauer beam incident on the crystal was 14 photons/s. Even though the incident beam was very weak, the diffracted signal was strong enough to produce a clear signal over the ~ 0.25 photons/s background noise of the scintillation detector.

To measure the absolute integrated intensity required knowing the total incident power P_0 (all 14.4 KeV photons/s) and f_s, the fraction of P_0 that was recoilless. The recoilless fraction of the source was computed from a measurement of the area of the absorption dip from an enriched stainless steel absorber, and we found that $f_s = 0.77$. To compare measured and calculated values of the integrated intensity, the calculated integrated intensity, $\int P(\theta)/P_0\, d\theta$, is computed as follows:

$$\int P(\theta)/P_0\, d\theta = f_s \int R(\theta) d\theta + (1 - f_s) \int R_0(\theta) d\theta, \tag{1}$$

where $R(\theta)$ is the reflectivity arising from both nuclear and electronic scattering, and $R_0(\theta)$ is the reflectivity from only electronic scattering. For electronically forbidden reflections such as the 777 in Fe_2O_3, $R_0(\theta)$ is of course zero, so the right hand side of Eq. (1) becomes simply $f_s \int R(\theta) d\theta$. Note that Eq. (1) is applicable whether dynamical or kinematic scattering theory is used.

Integrated intensity measurements were made on the 666 (electronically allowed) reflection and on the 777 (electronically forbidden) reflection by step scanning through the Bragg reflections using two source velocities; one corresponding to an energy that was on-resonance and the other off-resonance. The velocities corresponding to resonance energies in $^{57}Fe_2O_3$ were initially determined by Doppler scanning the absorption spectrum of powdered $^{57}Fe_2O_3$, and the velocities selected for on-resonance and off-resonance measurements of the 777 reflection were verified by performing energy scans at the peak of the reflection. These measurements were all made without an external magnetic field applied to the sample.

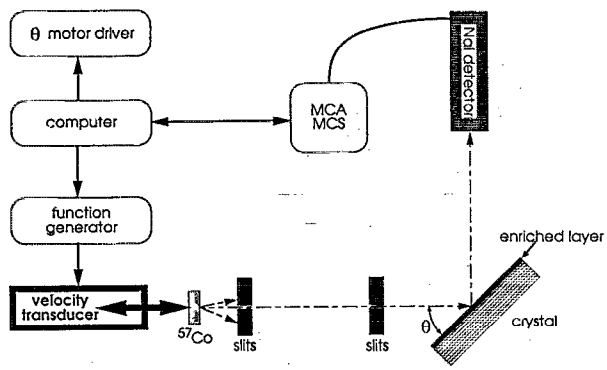

FIG. 2. Schematic of experimental setup used for diffraction measurements.

III. RESULTS

Figure 3(a) shows a step scanned diffraction profile of the 666 reflection for Doppler shifted photon energies of ± 11.88 mm/s, both of which are off-resonant energies. A diffraction peak is present at these off-resonant velocities since this reflection is allowed for both electronic and resonant nuclear scattering. Figure 3(b) shows similar diffraction measurements made at the 777 reflection for velocities that are on-resonance (8.39 mm/s) and off-resonance (-11.88 mm/s). There is a clear Bragg peak only for the on-resonance case since the 777 reflection is electronically forbidden. The data at 8.39 mm/s is actually an average over a ± 0.25 mm/s range centered at 8.39 mm/s. Despite the rather sizeable statistical uncertainties in the data of Fig. 3 (due to the low incident beam intensity), the distinction between on-resonance and off-resonance diffraction is clear for the 777 reflection. Because the Fe_2O_3 crystals have a mosaic spread of only ~ 15 arcs, the widths of the diffraction profiles in Fig. 3 are completely determined by the $\sim 0.2°$ angular width of the incident beam. The solid and dashed lines correspond to Gaussian fits to the measured data with the width constrained to the 0.2° incident beam divergence.

The measured integrated intensities are presented in Table I along with dynamical[1] and kinematic[20] calculated integrated intensities using the atomic form factors $f_{Fe}(666) = -9.303\text{-}i1.195$, $f_{Fe}(777) = -8.203\text{-}i1.195$, $f_O(666) = -1.811\text{-}i0.009$, and $f_O(777) = -1.621\text{-}i0.009$, and rhombohedral unit cell parameters $a_0 = 5.4348$ Å, and cosine of angle between lattice vectors of 0.570 24 ($V_c = 100.932$ Å^3). The Debye–

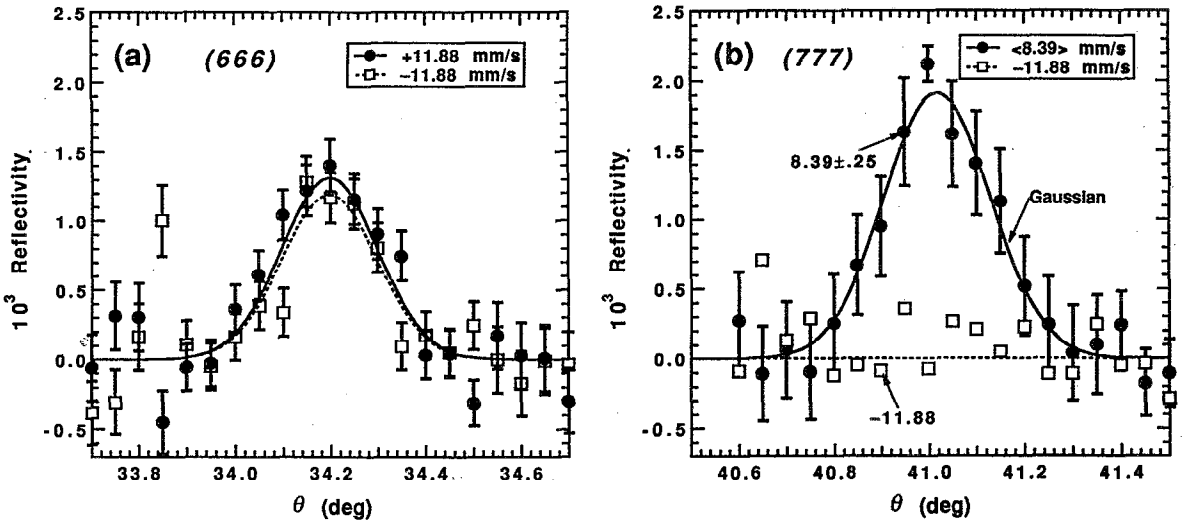

FIG. 3. Rocking curves used to get the absolute integrated intensity. (a) 666 reflection measured at ±11.88 mm/s, counted for 235 min/point; (b) 777 reflection at −11.88 mm/s and +8.39±0.25 mm/s, counted for 76 min/point.

Waller factors used are $B_{Fe} = 0.48$ and $B_O = 0.49$.[21] The measured integrated intensity of the 666 reflection lies between the dynamical and kinematic calculations, which indicates that the enriched $^{57}Fe_2O_3$ epitaxial layer is not ideally perfect; this is consistent with the observation of the ~15 arcs rocking curve width of the epitaxial layers. Off-resonance, at −11.88 mm/s, the very small (but nonzero) calculated value of the 777 integrated intensity demonstrates how rapidly the resonant scattering falls off with photon energy for electronically forbidden reflections. The uncertainties in the measured values listed in Table I represent the statistical uncertainties determined by the number of detected photons.

The photon energy dependence of the Bragg scattering at the 666 and 777 reflections is shown as a function of Doppler velocity in Fig. 4. This figure shows the measured energy dependence of the scattering as well as showing both kinematic and dynamic integrated intensity calculations. Since the angular width of the incident beam is more than 40 times the diffraction width of the crystal, it is appropriate to compare the observed scattering rate at the diffraction peak with integrated intensity calculations. The data in Fig. 4 have been scaled to absolute integrated intensities using the rocking curves from Fig. 3. Diffracted intensity is observed at all velocities for the electronically allowed 666 reflection shown in Fig. 4(a), while a reflection is observed only near resonant nuclear energies for the electronically forbidden 777 reflection in Fig. 4(b).

For the 666 reflection, the measured values [denoted by the open circles in Fig. 4(a)] lie between the kinematic and dynamical calculations. The thick solid line in the cross-hatched area is a linear combination of the dynamical and kinematic calculations given by r times the dynamical

TABLE I. Measured and calculated integrated intensity, $\int P(\theta)/P_0\, d\theta$ at 14.413 03 keV. The dynamical and kinematic columns are calculated values using Eq. (1). For the 666 reflection, $\int R_0(\theta)d\theta$ is 2.80×10^{-6} from dynamical theory, and 6.81×10^{-6} from kinematic theory.

hkl	Velocity (mm/s)	Measured	Dynamical	Kinematic
666	+11.88	$6.3\pm0.5\times10^{-6}$	3.21×10^{-6}	7.97×10^{-6}
666	−11.88	5.3±0.3	2.43	5.80
777	⟨+8.39⟩[a]	7.5±0.5	6.88	10.56
777	−11.88	0.5±0.5	0.05	0.07

[a]The velocity ⟨+8.39⟩ indicates that the associated integrated intensities are averaged over the range 8.39±0.25 mm/s.

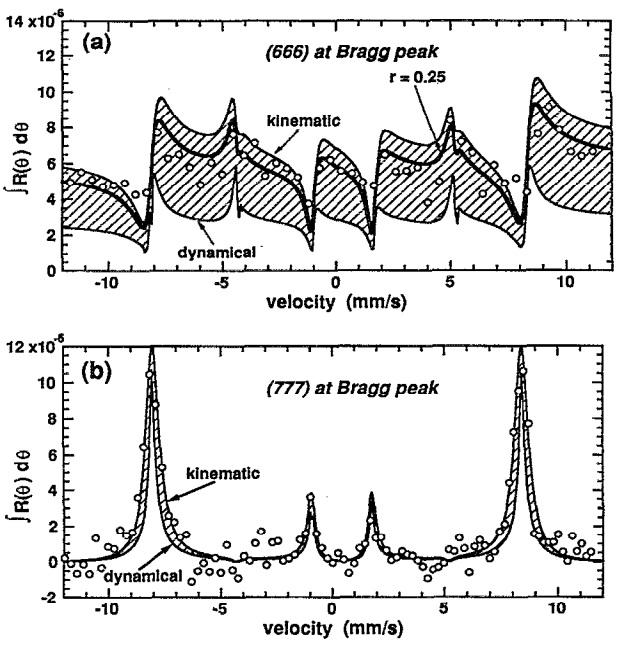

FIG. 4. Integrated intensity as a function of Doppler velocity showing the measured integrated intensity, dynamic calculation, and kinematic calculation. The shaded region is bordered by the dynamic and kinematic calculations, and the markers are the measured values. (a) 666 reflection measured for 234 h, the extra line marked r=0.25 is the linear combination of $r\times$(dynamic) + $(1-r)\times$(kinematic) calculations; (b) 777 reflection measured for 71 h.

calculation plus $(1-r)$ times the kinematic calculation. A value of $r=0.25$ was selected by requiring the linear combination to match the measurements in Table I at ± 11.88 mm/s, this indicates that the scattering is substantially kinematic. The oscillations as a function of source velocity that are visible in the measured data and the calculations arise from the resonant nuclear scattering and absorption. Even though these data have rather large statistical fluctuations, the general features of the energy profiles can be seen.

For the 777 reflection shown in Fig. 4(b), both the measurements and the calculations show that only four of the six resonant energy levels diffract. For this reflection the integrated intensities calculated using the dynamical and kinematic theories are so similar that the measurements cannot easily distinguish between them. However, the Doppler *widths* of the two strong peaks favor the kinematic calculation over the dynamical calculation. Both the measured and the calculated Doppler widths for the 777 reflection are much wider than the natural width of the state. The calculated Doppler widths of the diffracted peaks are 0.76 mm/s (37 neV) using kinematic theory and 0.43 mm/s (21 neV) using dynamical theory, while the natural width of the state is only $\Gamma = 0.097\,02$ mm/s (4.665 neV). Note that these Doppler widths refer to the integrated intensity, not the peak intensity of an incident plane wave, which would be still wider in energy.[12,13] The Doppler width of our data, 0.84 ± 0.2 mm/s (40 neV), is uncorrected for source broadening.

IV. DISCUSSION

The results presented here show that $^{57}Fe_2O_3$ crystals can be grown epitaxially with high perfection, and that these crystals have the expected resonant nuclear scattering properties. This point is significant because it demonstrates that Mössbauer monochromators, for obtaining ultra-high energy resolution x-ray beams from synchrotrons, can be produced without the experimental difficulties and expense of dealing with bulk quantities of the pure ^{57}Fe isotope. The integrated intensity measurements in Table I and the data in Fig. 4(b) indicate that the ~ 15 arcs mosaic widths of these crystals produce larger integrated intensities than would be obtained from perfect crystals. Larger integrated intensities are, of course, desirable for monochromators as long as the broader angular resolution is acceptable. The effect of the mosaic width on the performance of these crystals as resonant monochromators at synchrotrons will depend upon the angular width of the incident beam. For example, incident beams from sagitally focused monochromators can make use of at least part of the mosaic width, whereas beams premonochromated with very high order reflections will be weaker than those from a perfect $^{57}Fe_2O_3$ crystal. Preliminary studies (to be reported elsewhere) of the performance of these epitaxial crystals on sagitally focussing beam lines at the Cornell High Energy Synchrotron Source (CHESS) and the National Synchrotron Light Source (NSLS) show a factor of ~ 10 increase in total resonant intensity over perfect crystals and high resolution premonochromators.[16]

From the dynamic scattering calculations shown in Fig. 4(b), the Doppler widths of the diffracted resonance lines at the 777 reflection are computed to be 4.4Γ (Γ is the natural width of the resonance). This broadening, sometimes referred to as "speed up" due to its effect upon the time dependent scattering, is well known.[1,5] Doppler broadening during diffraction from $^{57}FeBO_3$ crystals has been studied using a high angular resolution geometry by van Bürck *et al.*[9–11] Their results show that the broadening is a strong function of the incident angle, and it can reach $\sim 20\Gamma$ at the reflectivity peak. When integrated intensities are considered (as in the present work), the broadening is averaged over all incident angles, and the resultant broadening is considerably less than 20Γ as is shown in Fig. 4(b).

Since the measured integrated intensities of the 666 reflection in Table I are greater than those given by the dynamical calculations, we infer that the characteristic sizes of the individual crystallites in the sample are smaller than the primary extinction length of the 666 reflection. That the measured intensities in Fig. 4(a) lie between the dynamical and kinematic calculations is qualitatively consistent with the ~ 15 arcs mosaic width of the epitaxial layer. That is, since the intrinsic Darwin width for these crystals is < 1 arcs, a significant departure from dynamic scattering conditions is expected. Although we have not yet attempted to grow more perfect epitaxial crystals by adjusting the crystal growing process, it is expected that better epitaxy can be produced either by varying the growth conditions or starting with more perfect substrate material. The rocking curve widths for the substrates used here were ~ 8 arcs, so the substrate was probably not the limiting factor.

V. CONCLUSIONS

We have grown epitaxial single crystals of $^{57}Fe_2O_3$ on natural Fe_2O_3 substrates using only a small quantity of enriched isotope, and we have investigated the resonant nuclear scattering properties of the crystals using a ^{57}Co radioactive source. Measurements of the energy dependent integrated Bragg intensity at the Mössbauer resonance show that the diffraction properties of the epitaxial layers lie between the dynamic and kinematic limits, qualitatively consistent with the measured mosaic of ~ 15 arcs. We conclude that enriched epitaxial crystals provide an alternative to the use of large amounts of expensive bulk isotope for monochromating synchrotron x-ray beams to submicrovolt bandwidths.

ACKNOWLEDGMENTS

The authors want to thank G. T. Trammel for helpful discussions and suggestions at the inception of this project. We also thank R. M. Moon for providing the hematite substrate, and W. E. Brundage for help in setting up the crystal growing apparatus, and advice on the method of crystal growth. This research was sponsored by the Division of Materials Sciences, U.S. Department of Energy un-

der Contract No. DE-AC05-84OR21400 with Martin Marietta Energy Systems, Inc.

[1] J. P. Hannon and G. T. Trammel, Phys. Rev. **186**, 306 (1969).
[2] Yu. Kagan, A. M. Afanas'ev, and I. P. Perstnev, Sov. Phys. JETP **27**, 819 (1968).
[3] A. M. Afanas'ev and Yu. Kagan, Sov. Phys. JETP **21**, 8215 (1965).
[4] Yu. Kagan and A. M. Afanas'ev, Sov. Phys. JETP **23**, 178 (1966).
[5] Yu. Kagan, A. M. Afanase'v, and V. G. Kohn, J. Phys. C **12**, 615 (1979).
[6] A. N. Artem'ev, I. P. Perstnev, V. V. Sklyarevskiĭ, G. V. Smirnov, and E. P. Stepanov, Sov. Phys. JETP **37**, 136 (1973).
[7] E. P. Stepanov, A. N. Artem'ev, I. P. Perstnev, V. V. Sklyarevskiĭ, and G. V. Smirnov, Sov. Phys.-JETP **39**, 562 (1974).
[8] A. V. Artem'ev, N. P. Perstnev, V. V. Sklyarevskiĭ, and E. P. Stepanov, Sov. Phys. JETP **46**, 587 (1977).
[9] U. van Bürck, H. J. Marus, G. V. Smirnov, and R. L. Mössbauer, J. Phys. C **17**, 2003 (1984).
[10] U. van Bürck, G. V. Smirnov, H. J. Marus, and R. L. Mössbauer, J. Phys. C **19**, 2557 (1986).
[11] U. van Bürck, G. V. Smirnov, R. L. Mössbauer, H. J. Marus, and N. A. Semioschkina, J. Phys. C **13**, 4511 (1980).
[12] M. Shvyd'ko and G. V. Smirnov, J. Phys. Condensed Matter **1**, 10563 (1989).
[13] U. van Bürck, G. V. Smirnov, R. L. Mössbauer, and Th. Hetrich, J. Phys. Condensed Matter **2**, 3989 (1990).
[14] E. Gerdau, R. Rüffer, R. Hollatz, and J. P. Hannon, Phys. Rev. Lett. **57**, 1141 (1986).
[15] U. van Bürck, R. L. Mössbauer, E. Gerdau, R. Rüffer, R. Hollatz, G. V. Smirnov, and J. P. Hannon, Phys. Rev. Lett. **59**, 335 (1987).
[16] G. Faigel, D. P. Siddons, J. B. Hastings, P. E. Haustien, and J. R. Grover, Phys. Rev. Lett. **58**, 2699 (1987).
[17] J. Arthur, G. S. Brown, D. E. Brown, and S. L. Ruby, Phys. Rev. Lett. **63**, 1629 (1989).
[18] *Crystal Growth an Introduction: International Summer School on Crystal Growth, 1971,* edited by P. Hartman (North-Holland, Amsterdam, 1973).
[19] H. Scholz and R. Kluckow, *Proceedings of International Conference on Crystal Growth, Boston, June, 1966,* edited by H. Steffen Peiser (Pergamon, New York, 1967).
[20] V. A. Belyakov, Sov. Phys.-Usp. **18**, 267 (1975).
[21] M. Brunel and F. de Bergevin, Acta Cryst. A **37**, 324 (1981).